Journal of Structural Biology **128,** 287–296 (1999)
Article ID jsbi.1999.4196, available online at http://www.idealibrary.com on IDEAL®

# Oligomerization State of MIP Proteins Expressed in *Xenopus* Oocytes as Revealed by Freeze-Fracture Electron-Microscopy Analysis

Patrick Bron,*,[1] Valérie Lagrée,* Alexandrine Froger,* Jean-Paul Rolland,* Jean-François Hubert,* Christian Delamarche,* Stéphane Deschamps,* Isabelle Pellerin,* Daniel Thomas,* and Winfried Haase†

**Equipe Canaux et Récepteurs Membranaires, UPRES-A CNRS 6026, Université de Rennes 1, Campus de Beaulieu, 35042 Rennes Cedex, Bretagne, France; and †Max-Planck-Institut für Biophysik, Heinrich-Hoffmann-Strasse 7, D-60528 Frankfurt am Main, Germany*

Received August 2, 1999, and in revised form September 30, 1999

**The MIP (major intrinsic protein) family is a widespread family of membrane proteins exhibiting two major types of channel properties: aquaporins and solute facilitators. In the present study, freeze-fracture electron microscopy was used to investigate the oligomerization state of two MIP proteins heterologously expressed in the plasma membrane of *Xenopus laevis* oocytes: AQPcic, an aquaporin from the insect *Cicadella viridis,* and GlpF, a glycerol facilitator from *Escherichia coli.* Swelling assays performed on oocytes 48 and 72 h following cRNA microinjections showed that these proteins were functionally expressed. Particle density determinations indicated that expression of proteins is related to an increase in particle density on the P fracture face of oocyte plasma membranes. Statistical analysis of particle sizes was performed on protoplasmic fracture faces of the plasma membrane of oocytes expressing AQPcic and GlpF 72 h after cRNA microinjections. Compared to control oocytes, AQPcic-expressing oocytes exhibited a specific population of particles with a mean diameter of 8.7 ± 0.1 nm. This value is consistent with the previously reported tetrameric organization of AQPcic. In addition, AQPcic particles aggregate and form orthogonal arrays similar to those observed in native membranes of *C. viridis,* consisting of homotetramers of AQPcic. On the protoplasmic fracture face of oocytes expressing GlpF, the particle density is increased by 4.1-fold and the mean diameter of specifically added particles is 5.8 ± 0.1 nm. This value fits with a monomer of the 28-kDa GlpF protein plus the platinum–carbon layer. These results clearly demonstrate that GlpF is a monomer when functionally expressed in plasma membranes of *Xenopus* oocytes and therefore emphasize the key role of the oligomerization state of MIP proteins with respect to their function.** © 1999 Academic Press

***Key Words:*** **freeze-fracture; electron microscopy; MIP family; oligomerization state; orthogonal array; *Xenopus* oocyte.**

## INTRODUCTION

The MIPs[2] (major intrinsic proteins) constitute a widespread membrane channel family that has been identified from bacteria to human. Two major functional subgroups of specific channels have been characterized: aquaporins (AQPs), which transfer water, and glycerol facilitators (GlpFs), which transfer glycerol and/or small neutral solutes. A third subgroup, a class of channels permeable to water, glycerol, and other small uncharged molecules, was recently described (Echevarria *et al.,* 1994; Ishibashi *et al.,* 1994, 1997; Ma *et al.,* 1994; Kuriyama *et al.,* 1997; Ishibashi and Sasaki, 1998; Tsukagushi *et al.,* 1998).

It is interesting to point out that many years prior to the molecular identification of water channels, special patterns of intramembrane particles observed by freeze-fracture electron microscopy were proposed to represent a morphological signature of water-transporting units (Chevalier *et al.,* 1974, 1979; Kachadorian *et al.,* 1975). Some aquaporins have already been reported to form orthogonal particle arrays. For instance, AQP4 and AQP0 form orthogonal arrays in various expression systems (Yang *et al.,* 1996; Van Hoek *et al.,* 1998; Ehring *et al.,* 1990; Verbavatz *et al.,* 1994).

Secondary structure predictions based on the highly conserved residues and short hydrophobic sequences led to a common structural model: MIP proteins exhibit six helical transmembrane segments with the N and C termini located in the

[1] To whom correspondence should be addressed. Fax: (33) 2 99 28 14 77. E-mail: Patrick.Bron@univ-rennes1.fr.

[2] Abbreviations used: MIP, major intrinsic protein; AQP, aquaporin; GlpF, glycerol facilitator; PF, protoplasmic fracture face; FC, filter chamber; POutA, particle outside aggregate; PInA, particle inside aggregate.



1047-8477/99 $35.00

cytoplasm (Jung *et al.,* 1994). The three-dimensional structure of AQP1 was resolved at 6-Å resolution by electron crystallography (Walz *et al.,* 1997; Cheng *et al.,* 1997; Li *et al.,* 1997) and seems to confirm the common structural model. The protein complex is made up of four monomers. Each monomer consists of six tilted α-helices spanning the membrane bilayer surrounding a central density area.

Few data exist about the oligomerization state of the MIP proteins. The eukaryotic AQP0 (Aerts *et al.,* 1990; König *et al.,* 1997), AQP1 (Smith and Agre, 1991; Verbavatz *et al.,* 1993), AQP2 (Kamsteeg *et al.,* 1999), AQPcic (Beuron *et al.,* 1995), and AQP4 (Verbavatz *et al.,* 1997) and the prokaryotic AqpZ (Ringler *et al.,* 1998) have been demonstrated to exist as homotetramers. Using velocity sedimentation on sucrose gradients, we have demonstrated that AQPcic, an insect aquaporin, and GlpF, the glycerol facilitator channel of *Escherichia coli,* have different behavior in nondenaturing detergents, indicating that glycerol facilitators could be monomers (Lagrée *et al.,* 1998b). These results suggest a relationship between oligomerization and transport selectivity. By using site-directed mutagenesis, we further showed that a 2-amino-acid substitution transforms an aquaporin into a glycerol facilitator. This functional switch is correlated with a monomerization of the protein (Lagrée *et al.,* 1999). Thus it appears that in MIP proteins, a close relationship exists between the function and the oligomeric state. Since aquaporins exhibited different single-channel water permeabilities and that some aquaporins could function as well as solute transporters (AQP3, AQP7, AQP8, and AQP9), Van Hoek *et al.* (1998), have proposed that various oligomeric structures might exist for different MIP members. Therefore structural information concerning the oligomeric state of MIP proteins in membranes is needed to elucidate the relationship between oligomerization and function.

Freeze-fracture electron microscopy has been widely used to identify integral membrane proteins in natural membranes or reconstituted in proteoliposomes. Moreover, a recent analysis of freeze-fracture images has shown that it is possible to correlate dimensions of particles with protein structure (Eskandari *et al.,* 1998). It was reported that oocytes expressing exogenous channel proteins displayed a much higher particle density in the plasma membrane than water-injected oocytes. Moreover, exogenously expressed channels appeared as particles only on the protoplasmic fracture face (PF) (Eskandari *et al.,* 1998; Zampighi *et al.,* 1995). The diameter of specific particles appearing in the PF of oocyte plasma membranes following expression of AQP1 was 8.75 nm. This size is consistent with the tetrameric assembly of the polypeptide as determined from high-resolution projection maps. This approach can therefore be used as a means to determine the oligomerization state of membrane proteins functionally expressed in *Xenopus* oocyte plasma membranes.

The purpose of this study was to analyze the morphology of AQPcic and GlpF proteins functionally expressed in the plasma membrane of *Xenopus* oocytes using freeze-fracture electron microscopy. We have measured the densities and the sizes of particles corresponding to functional AQPcic and GlpF proteins in membranes of *Xenopus laevis* oocytes. An important finding is that the particle size of GlpF is significantly lower than that of AQPcic. From this result, we conclude that GlpF is a monomer when functionally expressed in the plasma membrane of *Xenopus* oocytes. This direct observation is in good agreement with our previous finding of a monomeric functional form of GlpF.

## MATERIALS AND METHODS

*Water and glycerol transport assays.* Studies on osmotic water or apparent glycerol permeabilities of oocytes were performed as previously described (Lagrée *et al.,* 1999). Briefly, the AQPcic cRNA and GlpF cRNA were transcribed from pSP-AQPcic and pSP-GlpF vectors. The water or cRNA was microinjected into *X. laevis* oocytes of stage VI. For water permeability measurements, swelling was induced by a fivefold dilution of extracellular buffer A (82.5 mM NaCl, 2.5 mM KCl, 1 mM $CaCl_2$, 1 mM $MgCl_2$, 2 mM $NaHCO_3$, 10 mM Hepes/NaOH, pH 7.4). For apparent glycerol permeability measurements, control and injected oocytes were transferred at 20°C in an isoosmotic solution (buffer A) containing 140 mM glycerol. In both cases, swelling oocytes were monitored by videomicroscopy.

*Immunoblotting.* Total membranes of *Xenopus* oocytes were prepared as previously described (Lagrée *et al.,* 1999). Proteins separated by SDS–PAGE (Laemmli, 1970) were transferred onto a PVDF membrane (Lagrée *et al.,* 1998a) and then immunodetection was performed using polyclonal rabbit antibodies raised against the native AQPcic protein (Beuron *et al.,* 1995) or raised against a synthetic C-terminal peptide of GlpF (Lagrée *et al.,* 1999).

*Sample preparation and freeze-fracture.* After functional studies, control oocytes and oocytes expressing recombinant proteins were fixed between two glass slides and prepared for freeze-fracture electron microscopy as previously described (Zampighi *et al.,* 1995). Most fracture planes passed through the cytoplasm instead of following the plane of the plasma membrane. So, the protocol was slightly modified by manual removal of most of the vitellus. Thus, extensive PFs and EFs (exoplasmic fracture faces) of the plasma membrane were obtained and additional experimental procedures were more reproducible. Freeze-fracturing was performed with the Biotech 2000 freeze-fracture apparatus (Leybold-Heraeus, Cologne, Germany). Images were recorded at a nominal magnification of 20 000 using a CM208 Philips electron microscope at 80 kV.

*Measurement of freeze-fracture particles and data analysis.* For particle density and particle size determinations, measurements were performed from at least two PFs of membranes from at least two oocytes. Images of the PF were enlarged to a final magnification of 41 000 and digitized using a flatbed desktop scanner. For particle density measurements, a final pixel size of

1.3 nm was used. Particle densities were automatically determined using MACs, an image processing software program (Rolland *et al.,* 1997). For particle size measurements, a pixel size of 0.5 nm was used. The particle size was figured out by measuring the width of the particle perpendicular to the direction of the shadow. Results were plotted as frequency histograms (Eskandari *et al.,* 1998; Van Hoek *et al.,* 1998) that were fitted to a multiple Gaussian function

$$y = \sum_i \alpha_i \exp\left[-(x - \beta_i)^2/\sigma_i^2\right],$$

where $x$ is the particle size, and $y$ is the relative frequency for a given size. Each population of particles is given as mean ± standard deviation.

*Native membrane preparation and calculation of projection map.* Native membranes of filter chamber (FC) of *Cicadella viridis* were prepared as described by Hubert *et al.* (1989) with some slight modifications: membrane fractions were washed for 24 h in an alkaline buffer with a very slow stirring, and then membranes were kept at 4°C for 1 week in order to enhance the order of native 2D crystals of AQPcic. Native membranes of FC were negatively stained with 2% uranyl acetate and observed with a CM12 Philips electron microscope operating at 80 kV. Images were recorded at a nominal magnification of 35 000 and digitized at a 10-μm pixel size on the micrograph with a Leafscan 45 CCD-array microdensitometer. Image processing was performed using the MRC image analysis package (Crowther *et al.,* 1996) and the SPIDER software system (Frank *et al.,* 1981).

## RESULTS

### *Expression of Proteins in Oocytes and Functional Assays*

AQPcic and GlpF were transcribed *in vitro* from pSP-AQPcic and pSP-GlpF vectors. cRNAs were microinjected into the cytoplasm of *Xenopus* oocytes. Control oocytes are defined as water-injected oocytes. The presence of AQPcic and GlpF in the cell membranes was verified by Western blotting. As shown in Fig. 1, AQPcic and GlpF are not detected in control oocytes. At 48 and 72 h following cRNA injection both proteins are detected in the oocyte membrane fraction with a significant increase of protein expression from 48 to 72 h. To analyze the functional expression of AQPcic and GlpF in the plasma membrane of oocytes, cell osmotic water permeability ($P_f$) and the apparent glycerol permeability ($P'_{gly}$) were measured by swelling assays (Fig. 1). Forty-eight hours following cRNA injection, AQPcic-expressing oocytes exhibit a 15-fold increase of $P_f$ compared with control oocytes, whereas oocytes injected with GlpF cRNA do not show any $P_f$ increase. GlpF-expressing oocytes present a 2-fold increase of $P'_{gly}$ compared with control oocytes. No modification of the apparent glycerol permeability is detected in oocytes expressing AQPcic.

### *Freeze-Fracture*

On freeze-fracture images, the PF of control oocytes exhibits a population of dispersed particles (Fig. 2A). The appearance of the PF plasma membrane of AQPcic and GlpF-expressing oocytes 48 and 72 h after cRNA injection is shown in Fig. 3. In contrast to control oocytes, the PF of oocytes expressing AQPcic displays numerous large aggregates of particles. At 72 h after AQPcic cRNA microinjection, the size and the number of such aggregates strongly increased (Fig. 3B). Moreover, at 72 h these aggregates form well-ordered orthogonal arrays as shown on the computed diffraction pattern (Fig. 4). Such orthogonal arrays are never observed in the plasma membrane of control oocytes. GlpF-expressing oocytes exhibit scattered small particles distributed in the fracture face of the plasma membrane (Fig. 3C). At 72 h after GlpF cRNA injection the density of

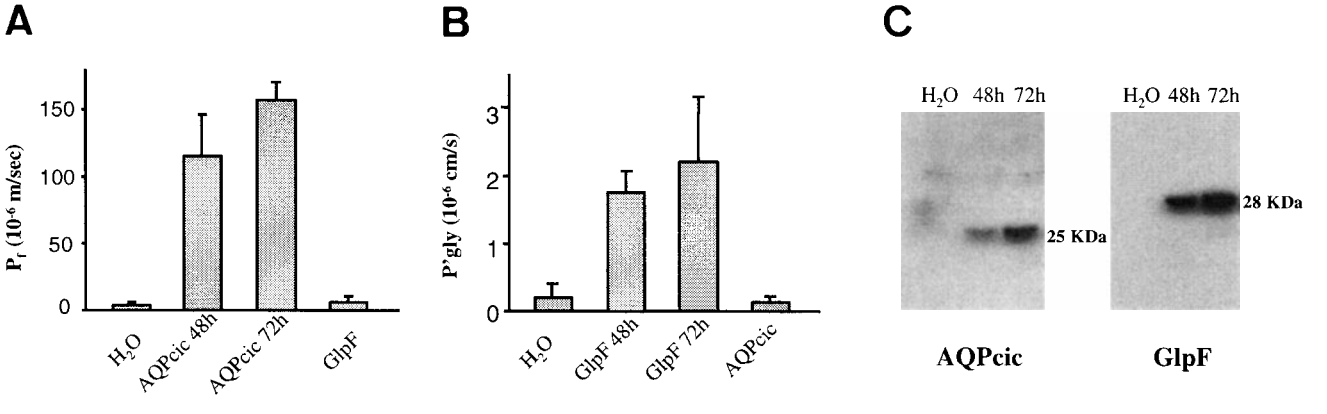


**FIG. 1.** Functional expression of AQPcic and GlpF in *Xenopus* oocyte membranes: (A and B) Results of swelling assays. Oocytes were injected with water, AQPcic cRNA, and GlpF cRNA. For water permeability ($P_f$) measurements, oocytes were exposed to an osmotic shock by a fivefold dilution of the extracellular buffer. For glycerol apparent permeability ($P'_{gly}$) measurements, oocytes were exposed to an isoosmotic buffer containing 140 mM glycerol. Swelling oocytes were monitored by videomicroscopy. Data are means ± SD. (C) Western blot analysis of membrane extracts from *Xenopus* oocytes injected with water, AQPcic cRNA, and GlpF cRNA. Immunodetections were achieved with anti-AQPcic antibodies (AQPcic) or with antibodies against a synthetic peptide of GlpF.

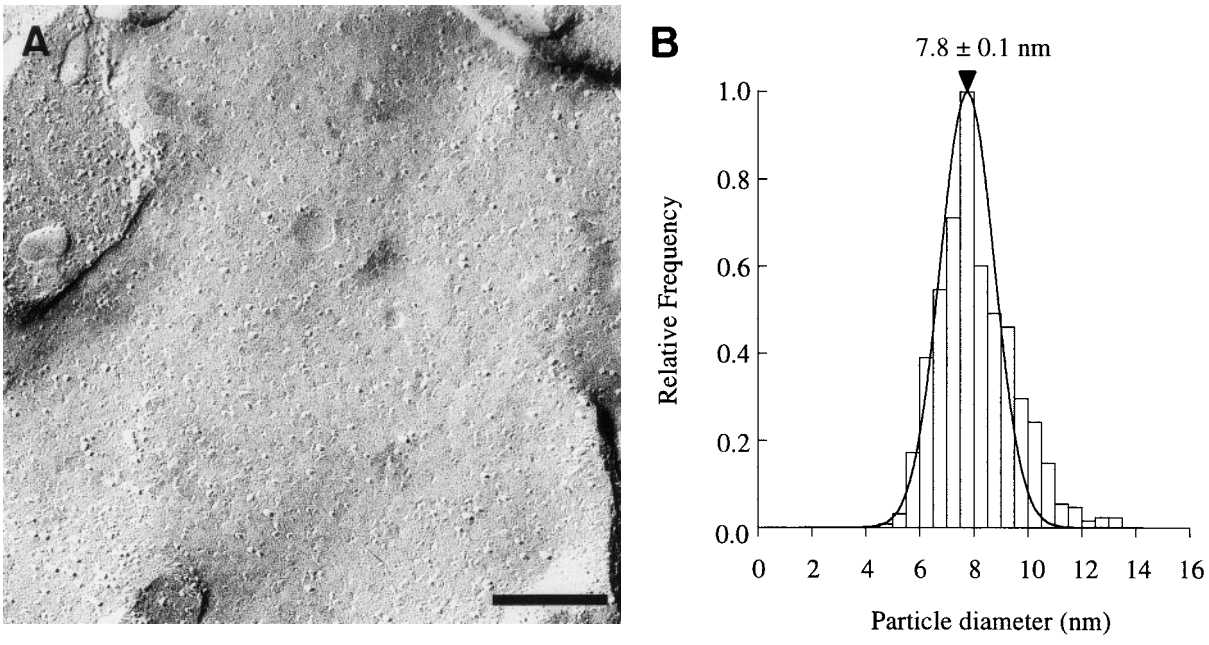


**FIG. 2.** Control oocytes 72 h following water injection: (A) PF of the control plasma membrane of *Xenopus laevis* oocytes 72 h after injection. The particle density is 346 ± 89 nm. (B) Frequency histogram of membrane particle sizes exhibits a Gaussian distribution of endogenous particles with a mean diameter of 7.8 ± 0.1 nm ($N$ = 674). Bar, 200 nm.

these particles is largely increased but no aggregates are observed (Fig. 3D).

*Particle Density*

Table I shows particle densities determined from the PF of oocytes injected with water, AQPcic, and GlpF cRNA at 48 and 72 h after injection. Particle densities reveal significant variations between control oocytes and AQPcic- and GlpF-expressing oocytes. Control oocytes do not exhibit a significant increase of particle density between 48 and 72 h. At 72 h the mean particle density is 346 particles/μm$^2$. AQPcic-expressing oocytes present numerous particle aggregates 48 h following cRNA injection. Thus, two types of measurements of particle densities were carried out: from particle inside aggregates (PInAs) and from particle outside aggregates (POutAs) (Table I). At 48 h the POutA density is slightly higher than that of particles from control oocytes but increases significantly after 72 h. The mean PInA density is 2267 ± 357 particles/μm$^2$ 72 h after cRNA injection. For orthogonal arrays, the center to center spacing for AQPcic particles is about 7.2 nm (Fig. 4); this gives a density of at least 19 290 particles/μm$^2$. Thus at 72 h, the density of particles for AQPcic-expressing oocytes is increased by 1.9- to 56-fold. In GlpF oocyte membranes, a significant increase in particle density is observed after 48 h when compared to control oocytes and a 4.1-fold increase of particle density is observed in GlpF-expressing oocytes at 72 h after injection.

*Particle Diameter*

Distributions of particle diameters are presented in Figs. 2B and 5. PFs of control oocytes exhibit a homogeneous distribution of particles with a mean diameter of 7.8 ± 0.1 nm. Expression of AQPcic is correlated with the appearance of densely packed proteins that can form orthogonal arrays. Two different frequency histograms of particle diameter from POutA and from PInA have been carried out (Figs. 5A and 5B). The frequency histogram determined on the PF from POutA (Fig. 5A) shows two populations of particles. One major population is observed of particles with a diameter of 7.3 ± 0.1 nm, similar to endogenous particles. A minor particle population is distinguished with a particle diameter of 8.2 ± 0.2 nm. A similar particle population is observed in the frequency histogram for PInA on the PF membranes (Fig. 5B). Indeed a homogeneous distribution of particles is observed with a mean diameter of 8.7 ± 0.1 nm. Oocytes expressing GlpF exhibit a bimodal distribution of particles, suggesting two major populations (Fig. 5C). The first population is composed of particles with a diameter similar to that of endogenous particles (7.8 ± 0.2 nm). The second population of particles displays a mean diameter of 5.8 ± 0.1 nm and is not present in the control oocytes.

*Projection Map of AQPcic*

To estimate the thickness of the platinum–carbon film, the accurate dimensions of AQPcic should be

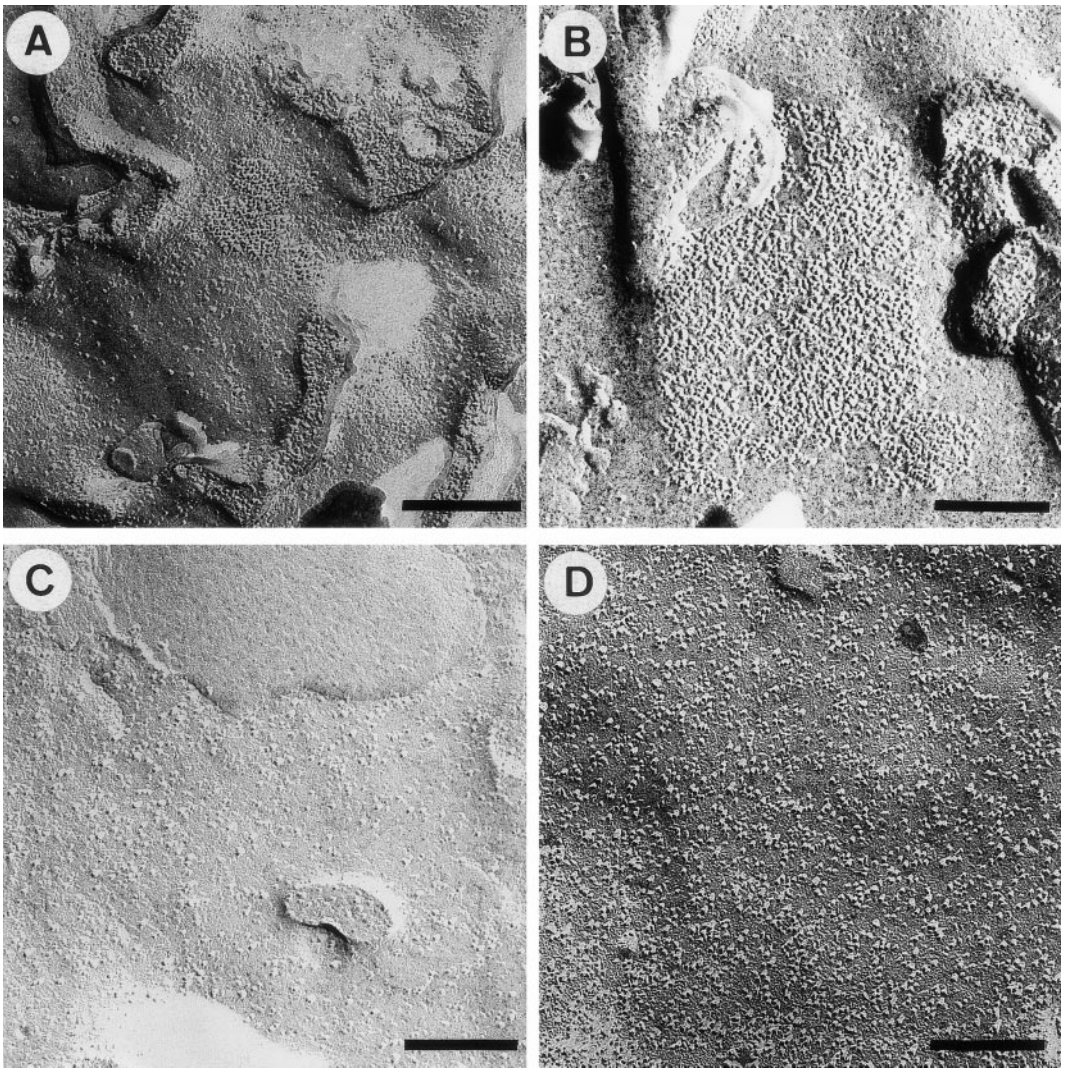


**FIG. 3.** Freeze-fracture electron micrographs of PF oocyte membranes 48 (A, C) and 72 h (B, D) following cRNA injection. (A and B) Replica from oocytes expressing AQPcic. AQPcic expression is correlated with the appearance of numerous large aggregates of particles. (C and D) Replica from oocytes expressing GlpF. GlpF expression is correlated with a significant increase of particle density 48 and 72 h following cRNA injection. In contrast to AQPcic, GlpF particles appear to be evenly distributed all over the oocyte membranes. Bars, 250 nm.

known. Therefore, a projection map of AQPcic was calculated at 15-Å resolution from negatively stained native two-dimensional crystals. Figure 6 shows a fully symmetrized projection map. From this map, we calculated a mean size for the AQPcic tetramer of 6.5 nm. This value corresponds to the average between the length of the edge (5.9 nm) and the diagonal of the tetramer (7.1 nm). The mean size of the AQPcic monomer is about 3 nm.

## DISCUSSION

Most integral membrane proteins are visible as intramembrane particles by freeze-fracture electron microscopy. In several studies it has been shown that it is possible to correlate the size of a freeze-fracture particle with the protein structure (Verbavatz *et al.,* 1993; Eskandari *et al.,* 1998; Van Hoek *et al.,* 1998). It has also been shown that variations in protein mass and glycosylation do not affect the particle diameter, but may modify the particle height. Thus, freeze-fracture electron microscopy can be used to determine the oligomerization state of heterologously expressed membrane proteins.

In the present study, two representative proteins of the two functional subgroups of the MIP family were investigated: AQPcic (Le Cahérec *et al.,* 1996a), an insect aquaporin that is nonglycosylated, and GlpF, the glycerol facilitator of *E. coli,* for which no report exists concerning any sugar association. Aquaporins and glycerol facilitators share similarities in their amino acid sequences and hydrophobicity pro-

files. So, the monomeric units are likely to exhibit similar structural organizations, but oligomerization state could vary in the different MIP class proteins. Subsequently, we expressed AQPcic and GlpF into *X. laevis* oocyte plasma membrane and investigated the size of corresponding particles by freeze-fracture electron microscopy.

Measurements of water and glycerol permeabilities of *Xenopus* oocytes expressing AQPcic and GlpF, as well as Western blotting, confirmed that functional proteins were expressed and delivered to the plasma membrane. In our experiments we found a $P_f$ of $170.10^{-6}$ cm/s 72 h after microinjection of AQPcic cRNA into oocytes. This value agrees well with the $P_f$ reported for AQP1 and AQPcic expressed in oocytes (Preston *et al.,* 1992; Le Caherec *et al.,* 1996a). In the same way, the glycerol permeability of oocytes expressing GlpF has been demonstrated. In both cases, functional activity increases from 48 to 72 h following cRNA microinjection.

Expression of AQPcic and GlpF resulted in a modification of the number and size of particles on the PF of the plasma membrane of oocytes as observed by freeze-fracture electron microscopy (Fig. 3). The size and density of intramembrane particles in the plasma membrane of AQPcic- and GlpF-expressing oocytes differed remarkably. While GlpF appears to be inserted evenly all over the oocyte membranes, AQPcic expression is related to the appearance of numerous particle aggregates. Indeed, 48 h after AQPcic cRNA injection into the cytoplasm of oocytes, numerous large aggregates of particles are found in the oocyte membranes. The number and the size of aggregates increase between 48 and 72 h following AQPcic cRNA injection (data not shown). For GlpF-expressing oocytes, 48 h after cRNA injection, there is a noticeable increase in particle density when compared to control oocytes and 72 h after cRNA injection a 4.1-fold increase in particle density is apparent. Consequently, our observations by freeze-fracture electron microscopy show clearly that the increase in channel activity is related to the appearance of particles on the PF of oocytes. These results confirmed previous data reported by Zampighi *et al.* (1995) and by Eskandari *et al.* (1998), verifying the assumption that exogenously expressed channel proteins appear as particles on the PF. In both cases, the appearance of particles is clearly more pronounced 72 h after cRNA injection (Figs. 3B and 3D). In addition, functional activities are slightly higher at 72 h than at 48 h after injection. Consequently, statistical analyses of particle sizes were performed on PF membranes 72 h after cRNA injection.

**TABLE I**
Particle Density 48 and 72 h Following Injection

| | 48 h | | 72 h | |
|---|---|---|---|---|
| | Particles/μm² | SD | Particles/μm² | SD |
| Control | 290 | ±39 (6) | 346 | ±89 (11) |
| AQPcic | | | | |
| POutA | 442 | ±58 (12) | 654 | ±208 (13) |
| PInA | 1445 | ±185 (4) | 2267 | ±357 (4) |
| GlpF | 482 | ±59 (17) | 1424 | ±211 (21) |

*Note.* Particle densities were determined from PF membranes of oocytes injected with water, AQPcic, and GlpF cRNA. Measurements were performed 48 and 72 h after injection. AQPcic-expressing oocytes present numerous densely packed proteins on PF membranes. Particle densities have been determined in two membrane areas: in areas that do not contain particle aggregates (particle outside aggregate, POutA) and in areas located inside aggregates (particle inside aggregate, PInA). SD, standard deviation. The number of PFs used for particle density measurements is given in parentheses.

Control oocytes exhibit a particle density of about 346 particles/μm² on PFs. Endogenous particles are homogeneously distributed in the PF of the membrane with a Gaussian distribution of a particle diameter of about 7.8 nm, which is consistent with a previously reported particle diameter for endogenous particles (Zampighi *et al.,* 1995; Eskandari *et al.,* 1998). The expression level of endogenous particles is similar to those previously reported. Zampighi *et al.* (1995) determined a density of particles on the PF of 212 particles/μm², whereas Eskandari *et al.* (1998) reported a density of 355 particles/μm². For uninjected oocytes, Bluemink *et al.* (1983) reported a density for endogenous intramembrane particles on the PF of 50 particles/μm².

On the PF of oocytes expressing AQPcic, two frequency histograms of the particle size have been calculated (Figs. 5A and 5B). The POutA PF exhibits a bimodal Gaussian distribution for the diameter of particles of 7.3 ± 0.1 and 8.2 ± 0.2 nm. The PInA PF

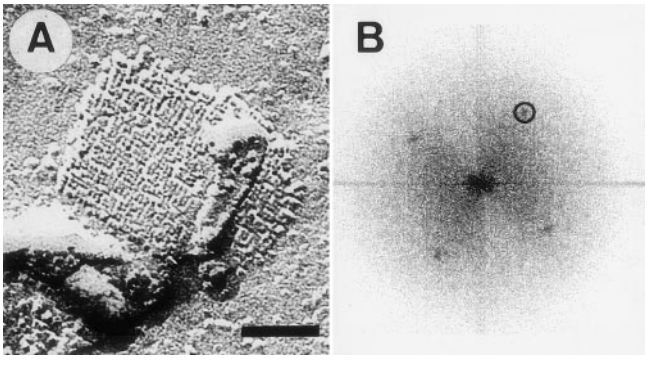


**FIG. 4.** Particle aggregates form orthogonal arrays. (A) PF membrane of an oocyte expressing AQPcic at 72 h following cRNA injection exhibits orthogonal array. (B) Diffraction pattern calculated from the image (A). The marked spot corresponds to a lattice spacing of 7.2 nm. Bar, 100 nm.

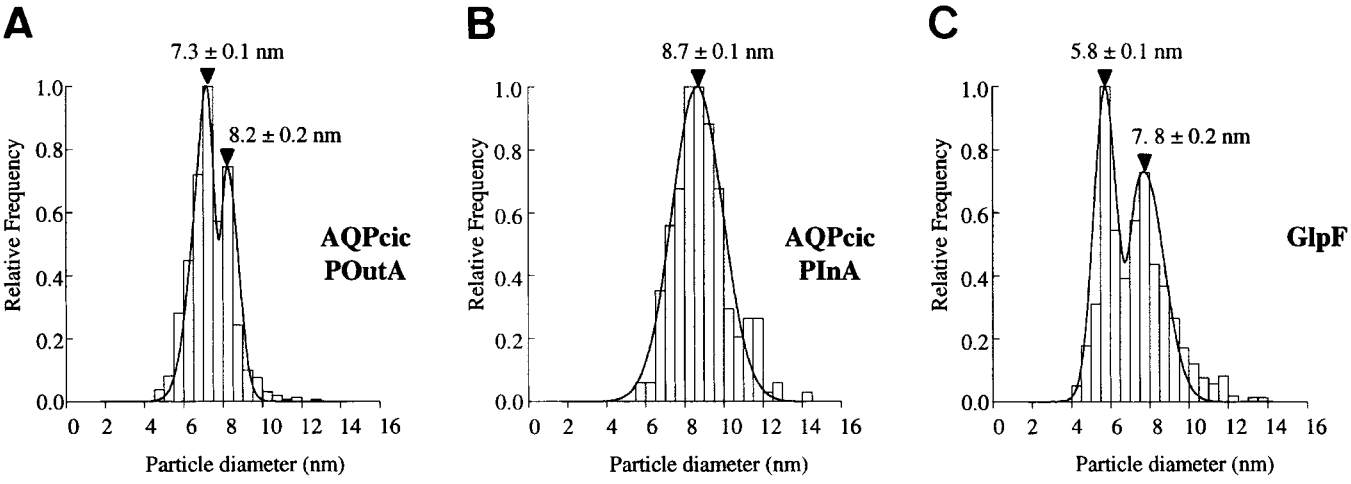


**FIG. 5.** Particle size distributions of PF membranes of oocytes expressing AQPcic and GlpF 72 h following injection. (A and B) Frequency histograms determined from membrane areas that do not contain particle aggregates (particle outside aggregate, POutA) and from membrane areas consisting of particle aggregates (particle inside aggregate, PInA) of AQPcic-expressing oocytes. (C) Frequency histogram determined from PF membranes of GlpF-expressing oocytes. Each frequency histogram represents the particle size distribution of one PF membrane: POutA ($N$ = 704 particles); PInA ($N$ = 308 particles); GlpF ($N$ = 853 particles).

reveals a single population of particles with a mean diameter of 8.7 nm. In comparison with control oocytes, the value of 7.3 ± 0.1 nm can be attributed to the endogenous particles. The large aggregates can organize into orthogonal arrays as seen in Fig. 4, similar to those previously observed in the native plasma membrane of the filter chamber of *C. viridis.* (Hubert *et al.,* 1989). Such particle aggregates were never seen in GlpF-expressing oocytes or in control oocytes. In P25 (the former name of AQPcic) incorporating proteoliposomes, tetrameric intramembrane particles similar to AQP1 were observed. Moreover these particles were often densely packed (Le Caherec *et al.,* 1996b). Also the average diameter of intramembrane particles measured in AQP1-reconstituted and freeze-fractured proteoliposomes was 8.5 ± 1.3 nm (Verbavatz *et al.,* 1993) and in oocytes expressing AQP1 a particle diameter of 8.9 nm was found (Eskandari *et al.,* 1998). Thus, since AQP1 and AQPcic are homotetramers, we could expect a par-

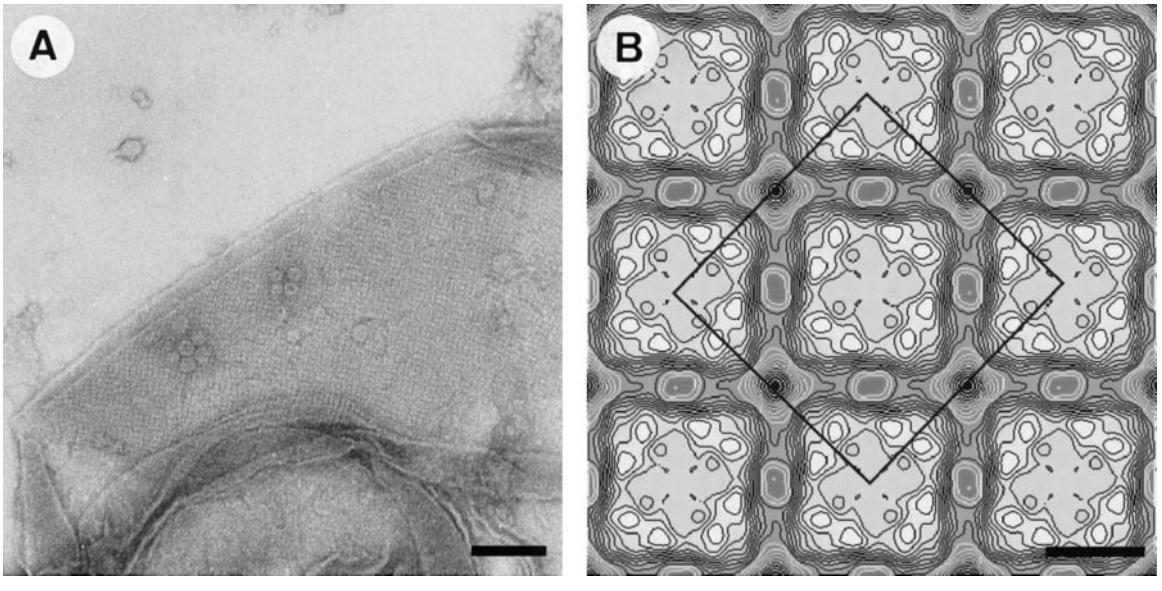


**FIG. 6.** Projection map of AQPcic from *C. viridis* at 15-Å resolution. (A) Electron micrograph of negatively stained filter chamber membranes with native crystals of AQPcic. Bar, 100 nm. (B) The fully symmetrized projection map at 15-Å resolution has been obtained from image processing of (A). Bar, 4 nm. AQPcic is a tetramer in which each monomer is composed of two unequal density domains. One unit cell with $a = b$ = 114 Å, $\gamma = 90°$ is outlined. The zero level was derived from the mean density of the map.

ticle size between 8.5 and 8.9 nm for AQPcic. In addition, in previous studies, sedimentation analysis of solubilized native protein and solubilized membrane proteins of oocytes expressing AQPcic revealed that AQPcic is expressed as a tetramer (Beuron *et al.,* 1995; Lagrée *et al.,* 1998b). These data strongly suggest that the particles of 8.7 nm observed in this study correspond to the AQPcic protein.

For the determination of the thickness of the platinum–carbon film deposited to produce the replicas, we have used AQPcic parameters derived from image processing. We modified the membrane preparation protocol in order to enhance the quality of the native 2D crystals of AQPcic. A projection map was obtained at 15-Å resolution from negatively stained specimens (Fig. 6B). This projection map allows new insights in the organization of AQPcic. It appears that each monomer is composed of two unequal density domains comparable to the peripheral protrusion lining the edges of the tetramer of AQP1 and AqpZ when analyzed by surface topography (Walz *et al.,* 1996; Scheuring *et al.,* 1999). The mean size of the AQPcic tetramer is about 6.5 nm and one monomer corresponds to 3 nm. The comparison of AQPcic particle diameter measured in freeze-fracture preparations and in our projection map allows us to estimate the platinum–carbon thickness at 1.1 nm.

For oocytes expressing GlpF 72 h following cRNA injection, the particles are evenly inserted into oocyte membranes. The measured density is 1424 particles/$\mu m^2$, which represents a 4.1-fold density increase. The size distribution reveals two populations of particles, with mean diameters of 5.8 and 7.8 nm, respectively. Compared to control oocytes, a new class of particles is observed at 5.8 nm. The 7.8-nm particle population is likely to correspond to the endogenous particles observed in control oocyte membranes and the 5.8-nm particles to the functional unit of GlpF, which corresponds to a diameter of 3.6 nm without the platinum–carbon layer. To address the question of the oligomeric state of the GlpF 3.6-nm particle, we have computed the average size for a 3-nm particle in various oligomeric states (Fig. 7). For a dimer, trimer, and tetramer, the expected average size should be 4.5, 6.0, and 6.5 nm, respectively. Thus, considering these possibilities, GlpF is likely to be a monomer, a dimer, or a combination of the two forms. If GlpF is a dimer, the thickness of the platinum–carbon would be 0.65 nm, which is 41% lower than calculated and seems unreasonable. If such variations in the thickness of the platinum–carbon film exist, we should observe significant variations in the particle diameter of GlpF-related particles according to the different freeze-fracture experiments. This is, however, not the case; thus such a variation of the thickness of the platinum–carbon film seems unlikely. Moreover, the low spread in diameter of the GlpF-related particle population and its corresponding mean diameter are not consistent with a mixed population of dimers and monomers even with a nonequal stoichiometry. Therefore, a 5.8-nm particle diameter for the monomer of GlpF unifies all our observations in a straightforward and self-consistent way.

In conclusion, this work presents a freeze-fracture microscopy approach in determining the oligomerization state of two representative proteins of the MIP family. AQPcic and GlpF expression led to morphological modifications of the plasma membrane of *X. laevis* oocytes with respect to number and size of intramembrane particles. A statistical analysis of the particle diameter was performed and indicated two new distinct populations of particles attributed to AQPcic and GlpF that allows us to conclude that *in situ* these proteins are tetrameric and monomeric, respectively. Taking into account the observation of Lagrée *et al.* (1998b, 1999) that a switch from the tetrameric to the monomeric organization was related to a change in transport specificity, we here provide an additional strong argument in favor of a functionality tightly correlated to the oligomerization state for the MIP family proteins.

We are indebted to Gorgette Bonnec for oocyte preparations, Joëlle Alory-Eury for photography, and Friederike Joos for assistance in freeze-fracture. This work was supported by La Fondation Langlois, Rennes, France.

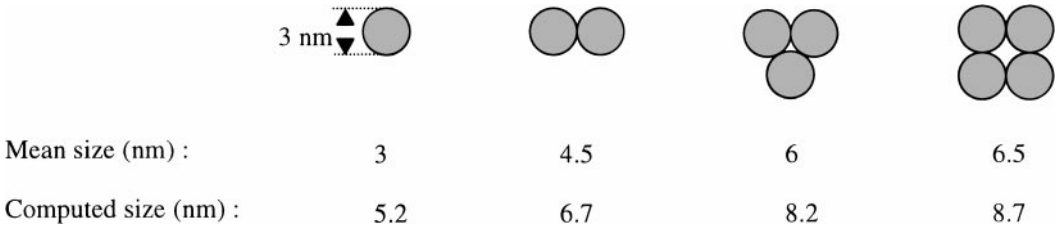


**FIG. 7.** Oligomeric models constructed from a monomeric unit with a mean diameter of 3 nm. The mean size is defined as the average value between the largest and the smallest dimensions of the model. The computed size corresponds to the mean size of the particle plus the platinum–carbon layer.

## REFERENCES


Aerst, T., Xia, J. Z., Slegers, H., De Block, J., and Clauwaert, J. (1990) Hydrodynamic characterization of the major intrinsic protein from the bovine lens fiber membranes, *J. Biol. Chem.* **265,** 8675–8680.

Beuron, F., Le Cahérec, F., Guillam, M. T., Cavalier, A., Garret, A., Tassan, J. P., Delamarche, C., Schultz, P., Mallouh, V., Rolland, J. P., Hubert, J. F., Gouranton, J., and Thomas, D. (1995) Structural analysis of a MIP family protein from the digestive tract of *Cicadella viridis, J. Biol. Chem.* **270,** 17414–17422.

Bluemink, J. G., Hage, W. J., Van Den Hoef, M. H. F., and Dictus, W. J. A. G. (1983) Freeze-fracture electron microscopy of membranes changes in progesterone-induced oocytes and eggs of *Xenopus laevis, Eur. J. Cell. Biol.* **31,** 85–93.

Cheng, A., Van Hoek, A. N., Yeager, M., Verkman, A. S., and Mitra, A. K. (1997) Three-dimensional organization of a human water channel, *Nature* **387,** 627–630.

Chevalier, J., Bourguet, J., and Hugon, J. S. (1974) Membrane associated particles: Distribution in frog urinary bladder epithelium at rest and after oxytocin treatment, *Cell Tissue Res.* **152,** 129–140.

Chevalier, J., Parisi, M., and Bourget, J. (1979) Particle aggregates during antidiuretic action. Some comments on their formation, *Biol. Cell.* **35,** 207–210.

Collaborative Computational Project 4. (1994) The CCP4 suite: Programs for protein crystallography, *Acta Crystallogr. Sect. D* **50,** 760–763.

Crowther, R. A., Henderson, R., and Smith, J.M. (1996) MRC image processing programs, *J. Struct. Biol.* **116,** 9–16.

Echevarria, M., Windhager, E. E., Tate, S. S., and Frindt, G. (1994) Cloning and expression of AQP3, a water channel from the medullary collecting duct of rat kidney, *Proc. Natl. Acad. Sci. USA* **91,** 10997–11001.

Ehring, G. R., Zampighi, G., Horwitz, J., Bok, D., and Hall, J. E. (1990) Properties of channels reconstituted from the major intrinsic protein of lens fiber membranes, *J. Gen. Physiol.* **96,** 631–664.

Eskandari, S., Wright, E. M., Kreman, M., Starace, D. M., and Zampighi, G. A. (1998) Structural analysis of cloned plasma membrane proteins by freeze-fracture electron microscopy, *Proc. Natl. Acad. Sci. USA* **95,** 11235–11240.

Frank, J., Shimkin, B., and Dowse, H. (1981) SPIDER—A modular software system for electron image processing, *Ultramicroscopy* **6,** 343–358.

Hubert, J. F., Thomas, D., Cavalier, A., and Gouranton, J. (1989) Structural and biochemical observations on specialized membranes of the "filter chamber," a water-shunting complex in sap-sucking homopteran insects, *Biol. Cell* **66,** 155–163.

Ishibashi, K., Kuwahara, M., Gu, Y., Kageyama, Y., Tohsaka, A., Suzuki, F., Marumo, F., and Sasaki, S. (1997) Cloning and functional expression of a new water channel abundantly expressed in the testis permeable to water, glycerol, and urea, *J. Biol. Chem.* **272,** 20782–20786.

Ishibashi, K., and Sasaki, S. (1998) The dichotomy of MIP family suggests two separate origins of water channels, *News Physiol. Sci.* **13,** 137–142.

Ishibashi, K., Sasaki, S., Fushimi, K., Uchida, S., Kuwahara, M., Saito, H., Furakawa, T., Nakajima, K., Yamaguchi, Y., Gojobori, T., and Marumo, F. (1994) Molecular cloning and expression of a member of the aquaporin family with permeability to glycerol and urea in addition to water expressed at the basolateral membrane of kidney collecting duct cells, *Proc. Natl. Acad. Sci. USA* **91,** 6269–6273.

Jung, J. S., Preston, G. M., Smith, B. L., Guggino, W. B., and Agre, P. (1994) Molecular structure of the water channel through aquaporin CHIP, *J. Biol. Chem.* **269,** 14648–14654.

Kachadorian, W. A., Wade, J. B., and Discala, V. A. (1975) Vasopresin: Induced structural change in toad bladder luminal membrane, *Science* **190,** 67–69.

Kamsteeg, E. J., Wormhoudt, T. A., Rijss, J. P., Van Os, C. H., and Deen, P. M. (1999) An impaired routing of wild-type aquaporin-2 after tetramerization with an aquaporin-2 mutant explains dominant nephrogenic diabetes insipidus, *EMBO J.* **18,** 2394–2400.

König, N., Zampighi, G. A., and Butler, P. J. (1997) Characterisation of the major intrinsic protein (MIP) from bovine lens fiber membranes by electron microscopy and hydrodynamics, *J. Mol. Biol.* **265,** 590–602.

Kuriyama, H., Kawamoto, S., Ishida, N., Ohno, I., Mita, S., Matsuzawa, Y., Matsubara, K., and Okubo, K. (1997) Molecular cloning and expression of a novel human aquaporin from adipose tissue with glycerol permeability, *Biochem. Biophys. Res. Commun.* **241,** 53–58.

Laemmli, U. K. (1970) Cleavage of structural proteins during the assembly of the head of bacteriophage T4, *Nature* **227,** 680–685.

Lagrée, V., Pellerin, I., Hubert, J. F., Tacnet, F., Le Cahérec, F., Roudier, N., Thomas, D., Gouranton, J., and Deschamps, S. (1998a) A yeast recombinant aquaporin mutant that is not expressed or mistargeted in *Xenopus* oocyte can be functionally analyzed in reconstituted proteoliposomes, *J. Biol. Chem.* **273,** 12422–12426.

Lagrée, V., Froger, A., Deschamps, S., Pellerin, I., Delamarche, C., Bonnec, G., Gouranton, J., Thomas, D., and Hubert, J. F. (1998b) Oligomerization state of water channels and glycerol facilitators. Involvement of loop E, *J. Biol. Chem.* **273,** 33949–33953.

Lagrée, V., Froger, A., Deschamps, S., Hubert, J. F., Delamarche, C., Bonnec, G., Thomas, D., Gouranton, J., and Pellerin, I. (1999) Switch from an aquaporin to a glycerol channel by two amino acids substitution, *J. Biol. Chem.* **274,** 6817–6819.

Le Cahérec, F., Deschamps, S., Delamarche, C., Pellerin, I., Bonnec, G., Guillam, M. T., Thomas, D., Gouranton, J., and Hubert, J. F. (1996a) Molecular cloning and characterization of an insect aquaporin. Functional comparison with aquaporin-1, *Eur. J. Biochem.* **241,** 707–715.

Le Cahérec, F., Bron, P., Verbavatz, J. M., Garret, A., Morel, G., Cavalier, A., Bonnec, G., Thomas, D., Gouranton, J., and Hubert, J. F. (1996b) Incorporation of proteins into (*Xenopus*) oocytes by proteoliposome microinjection: Functional characterization of a novel aquaporin, *J. Cell Sci.* **109,** 1285–1295.

Li, H., Lee, S., and Jap, B. K. (1997) Molecular design of aquaporin-1 water channel as revealed by electron crystallography, *Nat. Struct. Biol.* **4,** 263–265.

Ma, T., Frigeri, A., Hasegawa, H., and Verkman, A. S. (1994) Cloning of a water channel homolog expressed in brain meningeal cells and kidney collecting duct that functions as a stilbene-sensitive glycerol transporter, *J. Biol. Chem.* **269,** 21845–21849.

Mitra, A. K., Van Hoek, A. N., Wiener, M. C., Verkman, A. S., and Yeager, M. (1995) The CHIP28 water channel visualized in ice by electron crystallography, *Nat. Struct. Biol.* **2,** 726–729.

Preston, G. M., Carroll, T. P., Guggino, W. B., and Agre, P. (1992) Appearance of water channels in *Xenopus* oocytes expressing red cell CHIP28 protein, *Science* **256,** 385–387.

Ringler, P., Borgnia, M., Scheuring, S., Agre, P., and Engel, A. (1998) Two-dimensional crystals of a procaryotic water channel: AqpZ from *Escherichia coli, Biol. Cell.* **90,** 33–34.

Rolland, J. P., Bron, P., and Thomas, D. (1997) MACS: Automatic counting of objects based on shape recognition, *Comput. Appl. Biosci.* **13,** 563–564.

Scheuring, S., Ringler, P., Borgnia, M., Stahlberg, H., Müller, D. J., Agre, P., and Engel, A. (1999) High resolution AFM topographs of the *Escherichia coli* water channel aquaporin Z, *EMBO J.* **18,** 4981–4987.

Sigel, E. (1990) Use of *Xenopus* oocytes for the functional expression of plasma membrane proteins, *J. Membr. Biol.* **117,** 201–221.

Smith, B. L., and Agre, P. (1991) Erythrocyte $M_r$ 28 000 transmembrane protein exists as a multisubunit oligomer similar to channel proteins, *J. Biol. Chem.* **266,** 6407–6415.

Tsukagushi, H., Shayakul, C., Berger, U. V., Mackensie, B., Devidas, S., Guggino, W. B., Van Hoek, A. N., and Hediger, M. A. (1998) Molecular characterization of a broad selectivity neutral solute channel, *J. Biol. Chem.* **273,** 24737–24743.

Van Hoek, A. N., Yang, B., Kirmiz, S., and Brown, D. (1998) Freeze-fracture analysis of plasma membranes of CHO cells stably expressing aquaporins 1-5, *J. Membr. Biol.* **165,** 243–254.

Verbavatz, J. M., Brown, D., Sabolic, I., Valenti, G., Ausiello, D. A., Van Hoek, A. N., Ma, T., and Verkman, A. S. (1993) Tetrameric assembly of CHIP28 water channels in liposomes and cell membranes: A freeze-fracture study, *J. Cell. Biol.* **123,** 605–618.

Verbavatz, J. M., Van Hoek, A. N., Ma, T., Sabolic, I., Valenti, G., Ellisman, M. H., Ausiello, D. A., Verkman, A. S., and Brown, D. (1994) A 28 kDa sarcolemmal antigen in kidney principal cell basolateral membranes: Relationship to orthogonal arrays and MIP26, *J. Cell Sci.* **107,** 1083–1094.

Verbavatz, J. M., Ma, T., Gobin, R., and Verkman, A. S. (1997) Absence of orthogonal arrays in kidney, brain and muscle from transgenic knockout mice lacking water channel aquaporin-4, *J. Cell Sci.* **110,** 2855–2860.

Walz, T., Hirai, T., Murata, K., Heymann, J. B., Mitsuoka, K., Fujiyoshi, Y., Smith, B. L., Agre, P., and Engel, A. (1997) The three-dimensional structure of aquaporin-1, *Nature* **387,** 624–627.

Walz, T., Tittmann, P., Fuchs, K. H., Müller, D. J., Smith, B. L., Agre, P., Gross, H., and Engel, A. (1996) Surface topographies at subnanometer-resolution reveal asymmetry and sidedness of aquaporin-1, *J. Mol. Biol.* **264,** 907–918.

Walz, T., Typke, D., Smith, B. L., Agre, P., and Engel, A. (1995) Projection map of aquaporin-1 determined by electron crystallography, *Nat. Struct. Biol.* **2,** 730–732.

Yang, B., Brown, D., and Verkman, A. S. (1996) The mercurial insensitive water channel (AQP-4) forms orthogonal arrays in stably transfected Chinese hamster ovary cells, *J. Biol. Chem.* **271,** 4577–4580.

Zampighi, G. A., Kreman, M., Boorer, K. J., Loo, D. D. F., Benazilla, F., Chandy, G., Hall, J. E., and Wright, E. M. (1995) A method for determining the unitary functional capacity of cloned channels and transporters expressed in *Xenopus laevis* oocytes, *J. Membr. Biol.* **148,** 65–78.